Science Advances

AAAS

advances.sciencemag.org/cgi/content/full/3/5/e1700933/DC1

Supplementary Materials for

Structures of closed and open conformations of dimeric human ATM

Domagoj Baretić, Hannah K. Pollard, David I. Fisher, Christopher M. Johnson, Balaji Santhanam, Caroline M. Truman, Tomas Kouba, Alan R. Fersht, Christopher Phillips, Roger L. Williams

Published 10 May 2017, *Sci. Adv.* **3**, e1700933 (2017)
DOI: 10.1126/sciadv.1700933

The PDF file includes:

- References (*51–58*)

Other Supplementary Material for this manuscript includes the following:
(available at advances.sciencemag.org/cgi/content/full/3/5/e1700933/DC1)

- movie S1 (.mov format). Open and closed conformations of ATM.

Supplementary Materials

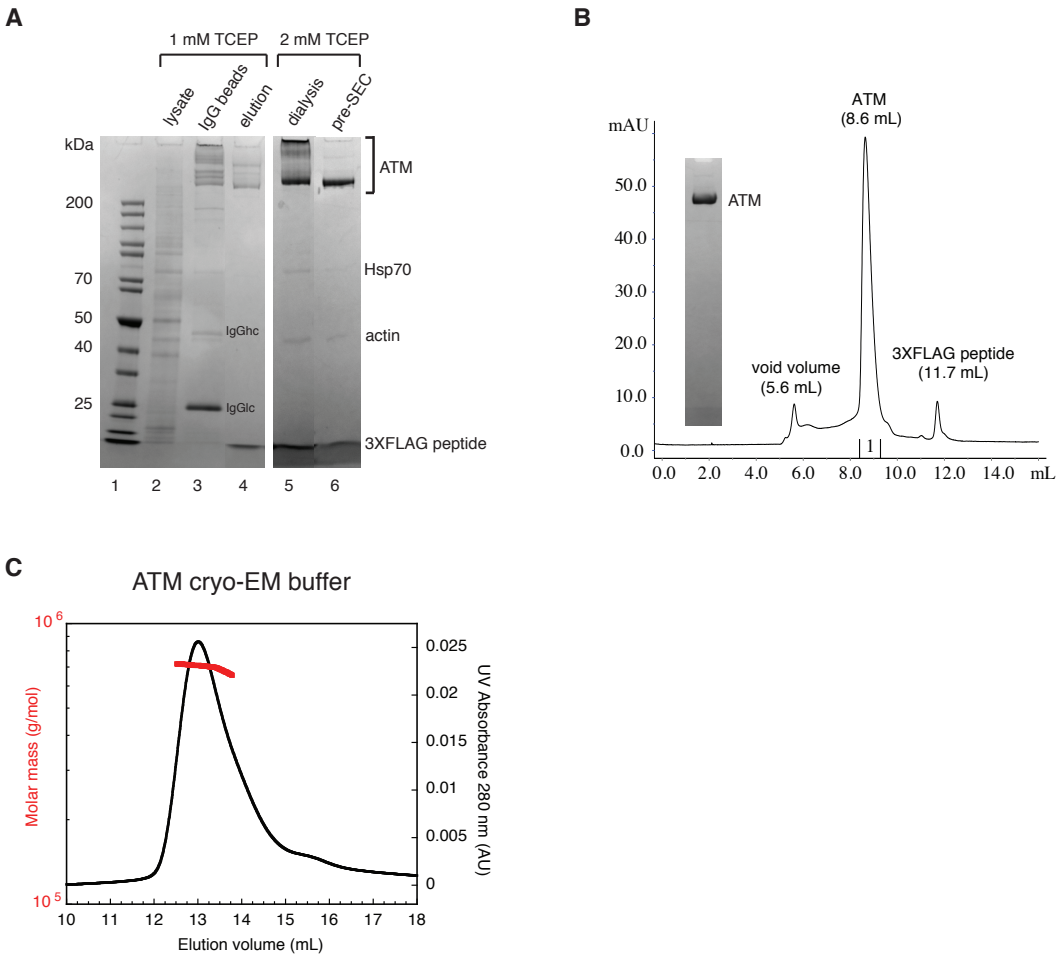

fig. S1. Purification of recombinant human ATM. (**A**) Affinity purification and dialysis of FLAG-tagged ATM. The SDS-PAGE Coomassie-stained gel shows: MW standard (lane 1), cell lysate supernatant (1:30 dilution) (lane 2), protein bound to the anti-FLAG IgG resin with the IgG heavy (hc) and light (lc) chains present (lane 3), 3XFLAG peptide eluted protein (lane 4), concentrated protein after overnight dialysis in strongly reducing conditions, 2 mM TCEP (lane 5), dialysed concentrated protein after removing larger aggregates by centrifugation before purification by the size-exclusion chromatography (SEC) (lane 6). Squared bracket indicates various ATM species detected by mass-spectrometry (MS) after the affinity purification and dialysis. Human chaperone Hsp70 and human actin were detected by MS as contaminants preceding the purification by SEC. (**B**) Size-exclusion chromatography of ATM on a TSKGel G4000SWXL column. The inset shows an SDS-PAGE Coomassie-stained gel of the peak fraction with a retention volume of 8.6 mL (collected as fraction 1). (**C**) Analysis of the molecular mass of the purified ATM by SEC using a Superose 6 10/300 column coupled to MALS (Multi-angle light scattering) detectors. The analysis indicates that the average molecular mass of the material corresponds to 700 kDa across the main peak of the chromatogram (red line). The expected molecular mass of the ATM dimer is 705 kDa. This suggests that ATM is a monodisperse dimer.

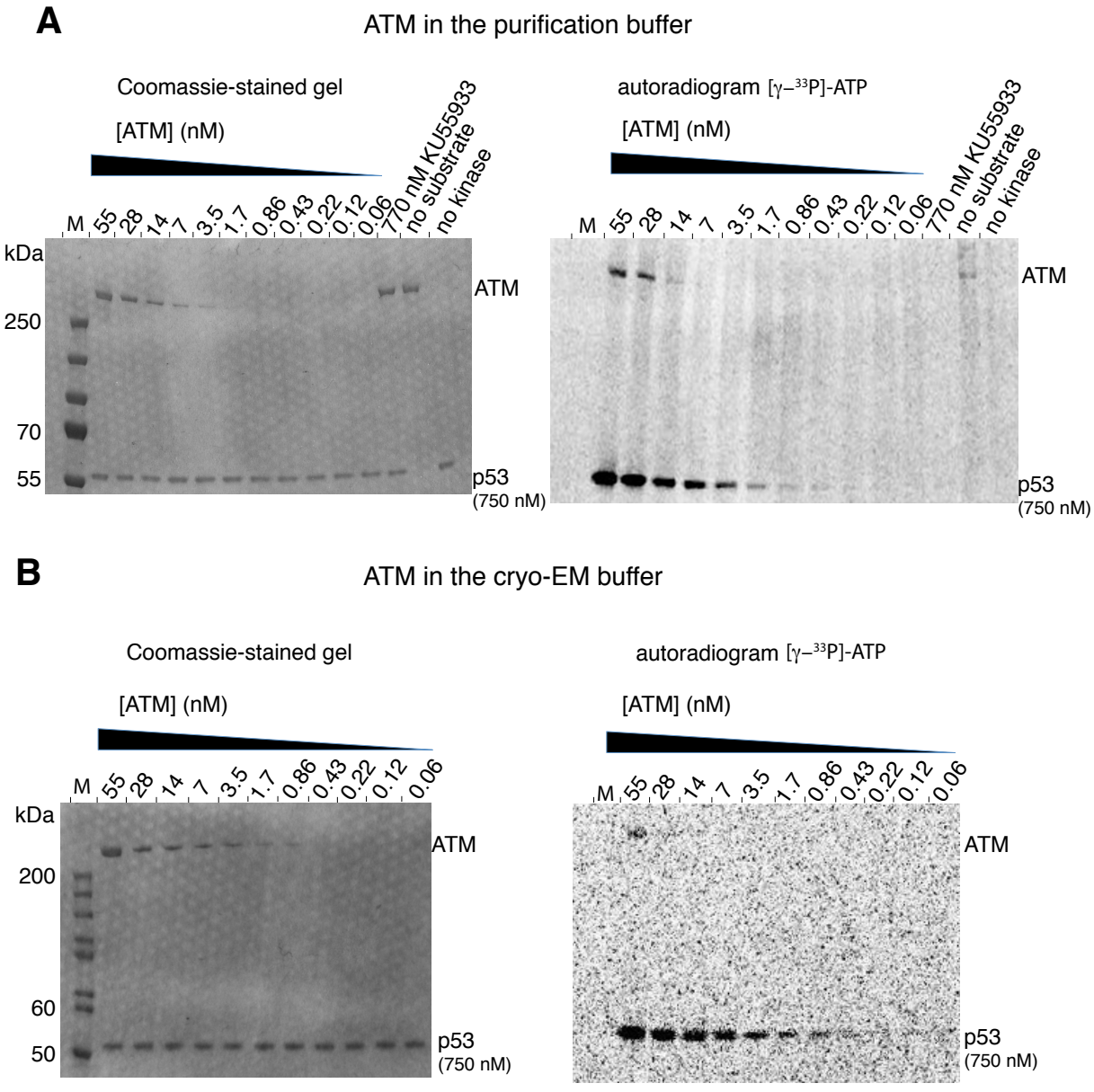

C

Modification	p53 peptide sequence	m/z (observed)	Charge state	Molecular mass/Da	Parent error/ppm	Mascot ion score
S15 phosphorylation	(Q)SDPSVEPPL**S**QETFSDLWK(L)	1,121.50	2+	2,240.99	-1.0	57

fig. S2. Recombinant human ATM is catalytically active. Phosphorylation of a full-length p53 substrate as a function of enzyme concentration was visualized by ^{33}P autoradiography. The ATM-specific inhibitor KU55933 (*51*) greatly reduces the enzymatic activity. (**A**) The reaction was performed in 50 mM HEPES pH 7.5, 150 mM NaCl, 10% glycerol and 2 mM TCEP buffer. (**B**) The reaction was performed in the conditions used for cryo-EM grid preparation (25 mM HEPES pH 7.5, 25 mM Tris pH 8.8, 150 mM NaCl, 0.01% Tween 20 and 2 mM TCEP buffer). (**C**) ESI-MS/MS analysis indicates that p53 is phosphorylated on S15.

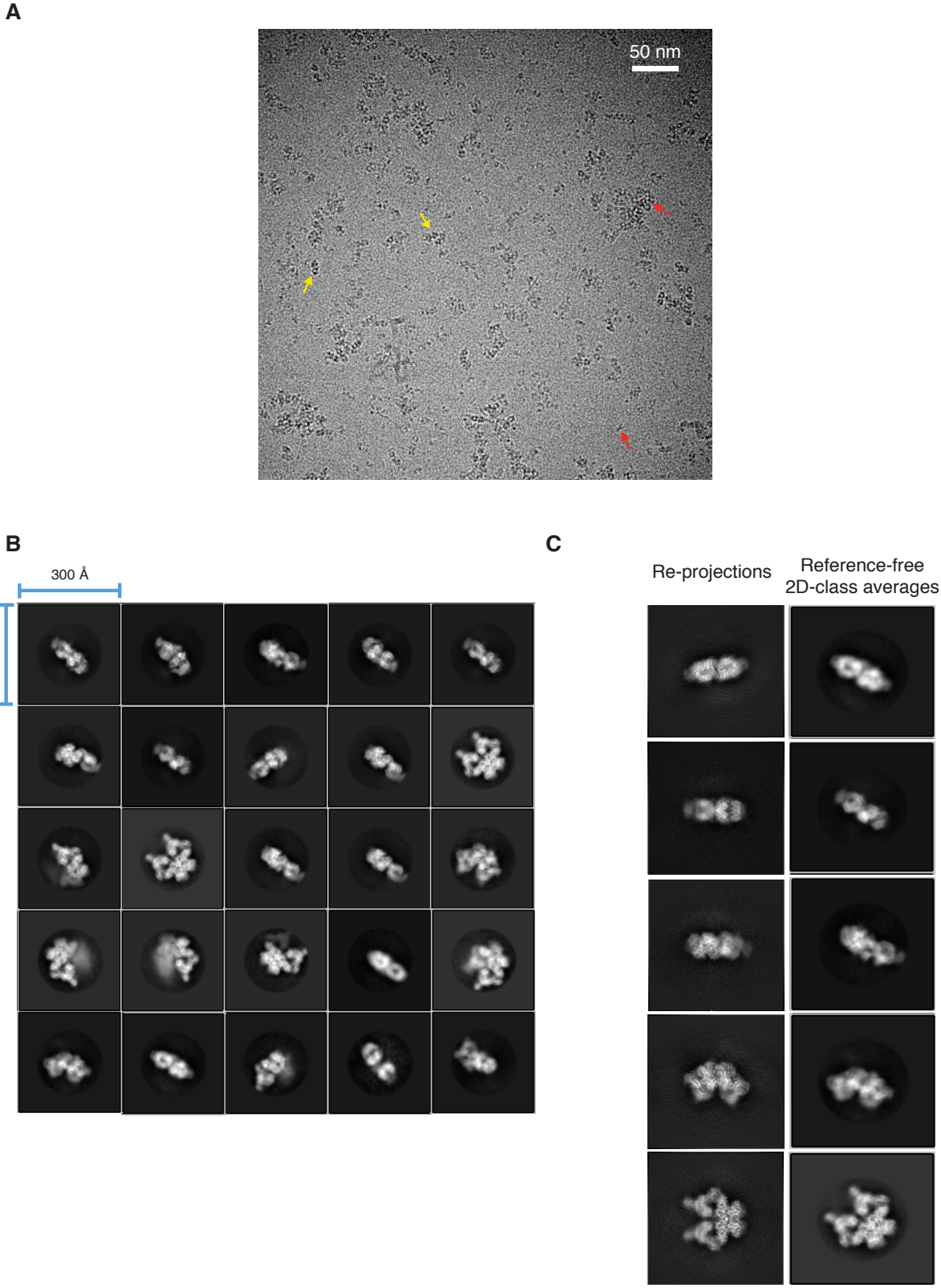

fig. S3. Cryo-EM images and 2D classes. (**A**) A typical micrograph of ATM particles in vitrified ice taken by the K2-summit camera. The yellow arrows indicate examples of the dimer particles included in the data processing. The red arrows point either to the typical larger aggregated particles or to a smaller damaged particle that were excluded from the final reconstruction. A scale bar is indicated in the upper right corner. (**B**) 2D-class averages of ATM included in the 3D volume reconstructions with the box size indicated. Displayed in Relion-1.4. (**C**) Re-projections (created by Relion) of the 3D volume (left) and matching reference-free 2D class averages (right).

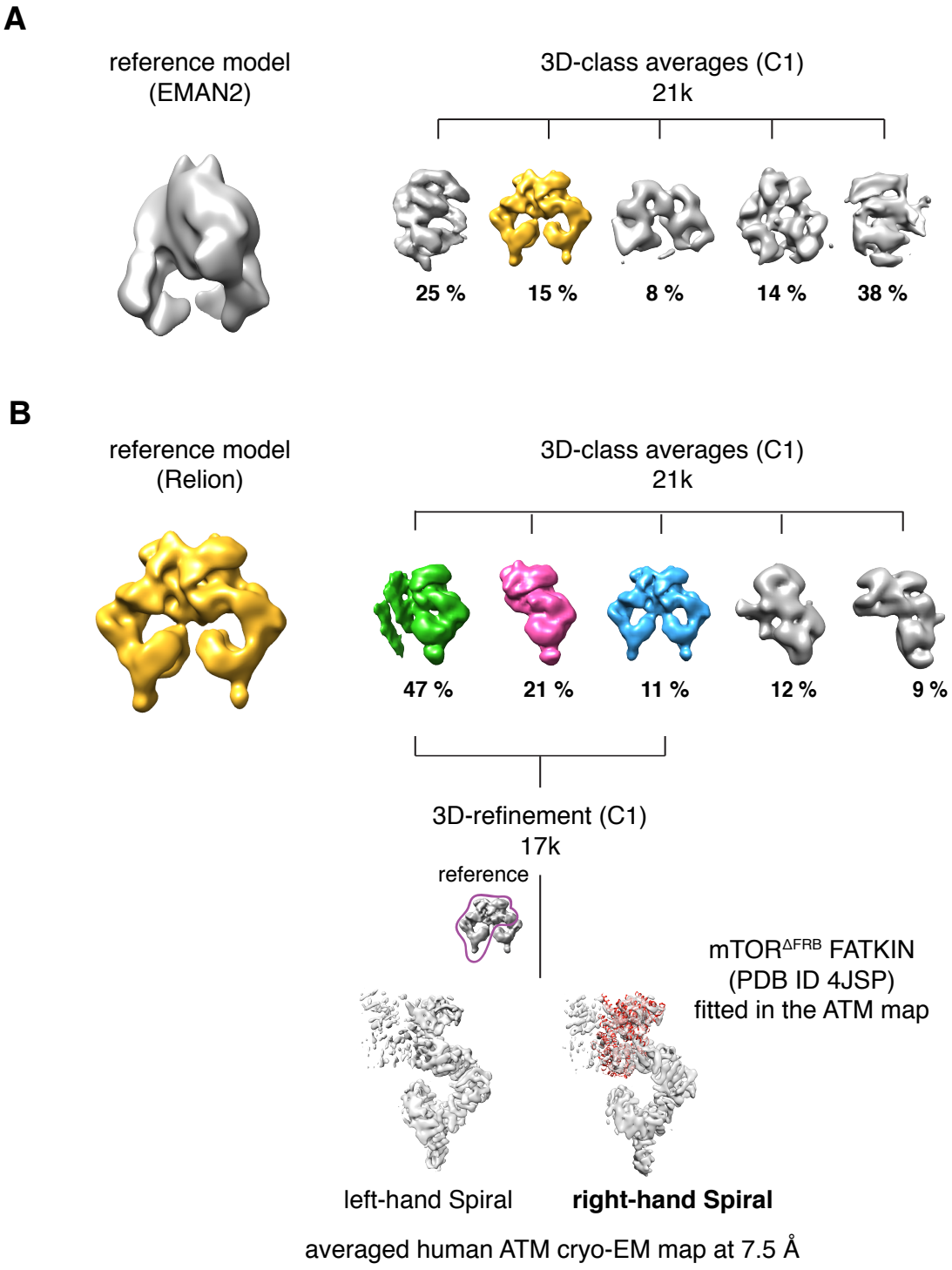

fig. S4. Reference models and 3D classes of human ATM. (**A**) The reference model generated by EMAN2 used for the initial 3D-classification (left). The resulting 3D classes with no symmetry imposed (C1) are illustrated (right). The class with the highest similarity to the experimental 2D projections was used as the reference model for further 3D classification and is colored in yellow. (**B**) The second cycle of 3D classification using the reference model obtained in (**A**). The three best classes (colored green, magenta and blue) were combined and refined to 7.5 Å using a mask around about 3/4 of the reference volume (illustrated with a purple curve). The hand of the ATM cryo-EM map was determined by manually fitting the mTOR FATKIN model (PDB ID 4JSV with the FRB domain deleted).

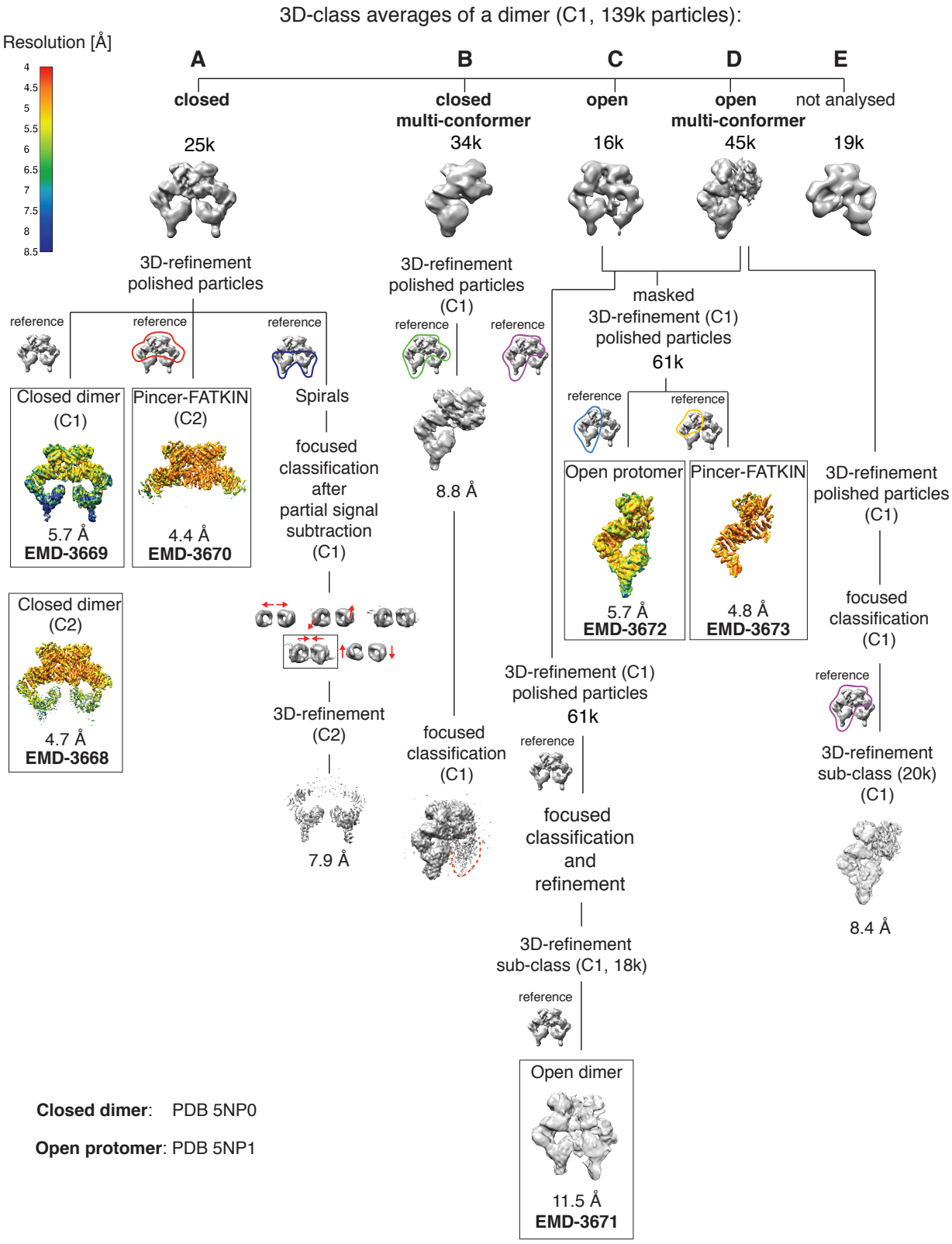

fig. S5. Summary of the cryo-EM 3D classification and focused refinement of ATM structures. A sum of 139k particles were classified into four distinct 3D-classes representing: **A** - the closed dimer (25k particles), **B** - the closed multi-conformer dimer (34k particles), **C** - the open dimer (16k particles) and **D** - the open multi-conformer dimer

(45k particles). The remaining 3D class with 19k particles (**E**) was excluded from the data analysis. The closed dimer (**A**) was the best class with C2 symmetry. This was refined to 4.4 Å with a mask encompassing the Pincer-FATKIN region and C2 symmetry imposed (EMD-3670). The same 3D-class was refined with a mask around the entire volume of a closed dimer at either 4.7 Å (C2 symmetry imposed, EMD-3668) or 5.7 Å (no symmetry, C1, EMD-3669). The independent movement of the Spiral domains (shown with red arrows) of the closed dimer was revealed by focused 3D classification after subtracting signal for the Pincer-FATKIN region. The best class of the Spirals (grey rectangle) was refined to 7.9 Å. For the closed multi-conformer dimer (**B**), the density for a disordered arm (highlighted with a red dashed curve) became more pronounced after focused 3D-classification. The 3D-class of the open dimer (**C**) was refined to 11.5 Å (EMD-3671). We combined 3D-classes for the open dimer (**C**) with the open multi-conformer dimer (**D**) in a masked refinement of either the open protomer at 5.7 Å (EMD-3672) or the open Pincer-FATKIN fragment at 4.8 Å (EMD-3673). The open multi-conformer dimer class (**D**) was further sub-classified and refined to 8.4 Å (20k particles). The local resolution of the closed dimer (arising from 3D class **A**) and the open protomer (arising from 3D classes **C** and **D**) final cryo-EM maps were calculated by the program ResMap(*52*). The colored curves around the reference template icons illustrate the regions that were masked in the course of refinement. For each refinement, the reference template was 3D class **A** (the closed dimer). Reconstructions deposited in wwPDB OneDep System are highlighted by squares. PDB codes of the deposited coordinates are indicated.

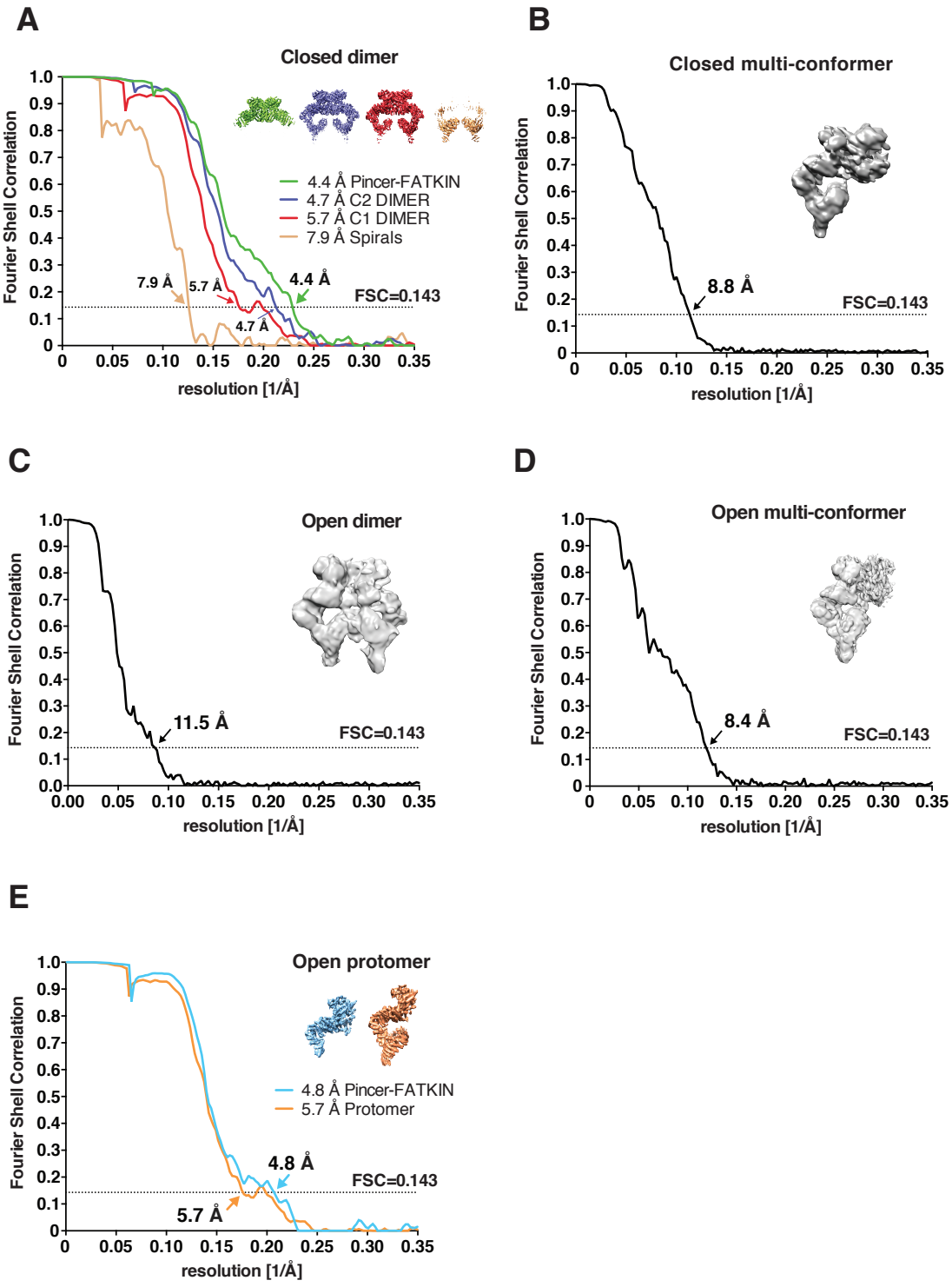

fig. S6. FSC curves for the observed reconstructions. FSC between two independently refined half-maps plots showing the overall resolution of the ATM maps reconstructed in this study (**A**-**E**).

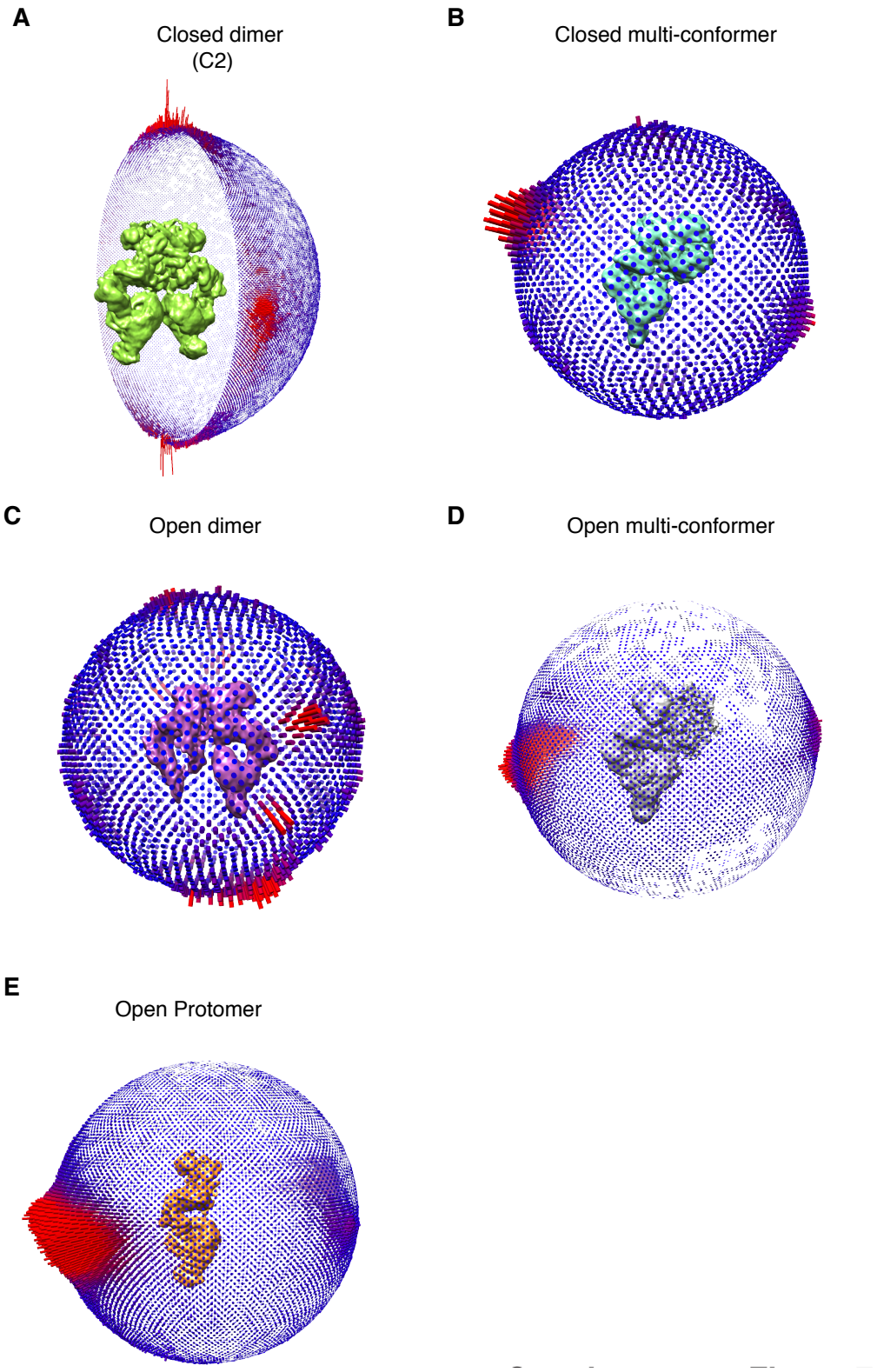

fig. S7. Euler angle distribution of particles for each 3D class (**A** to **E**). The angles are with respect to the reference volume assigned by RELION(*43*). The heights and colors of spikes emerging from spheres (visualized with UCSF Chimera(*53*)) both relate to the fraction of particles with a given orientation. Blue spikes represent orientations not commonly observed, and red spikes are the most common. The spikes are colored continuously from blue to red denoting -5σ to +5σ.

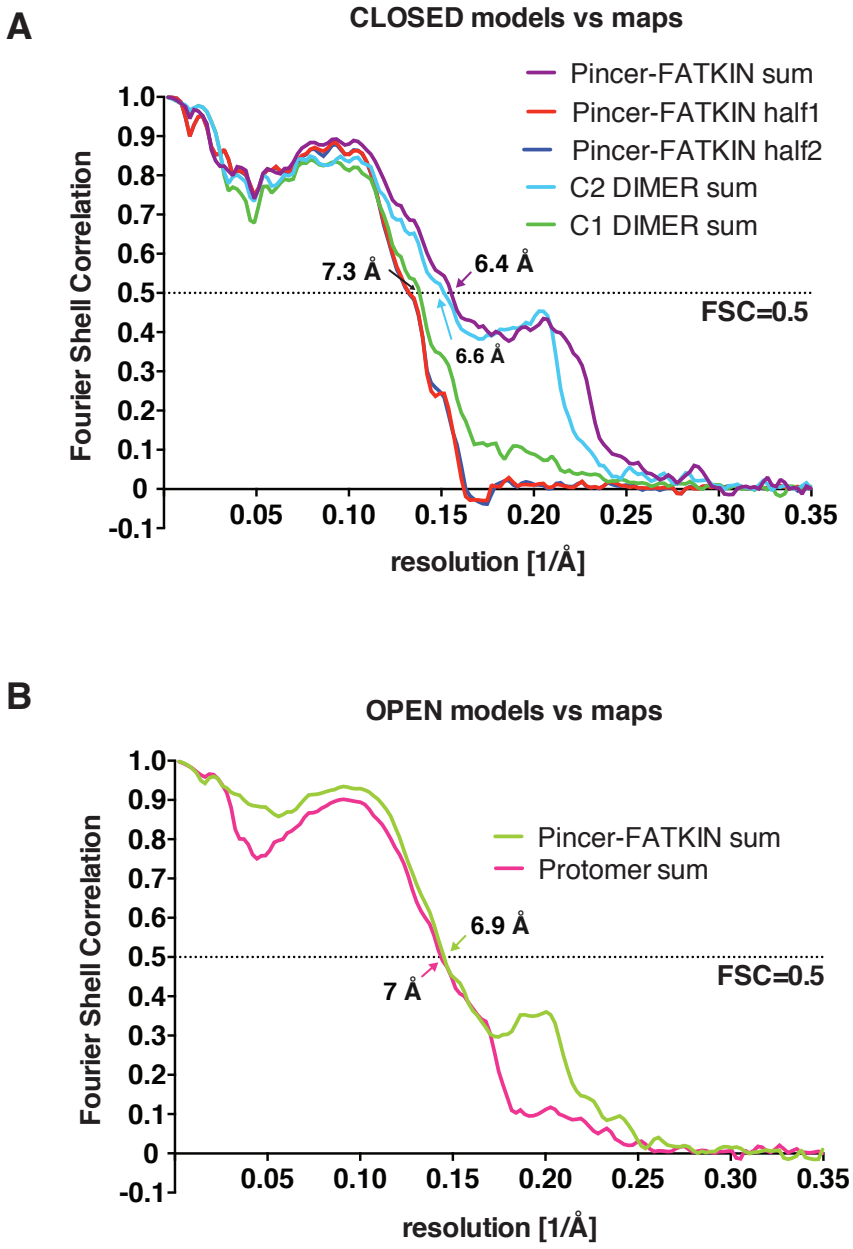

fig. S8. FSC between the ATM models and EM density maps.
(**A**) FSC curves for the closed models versus the unsharpened sum of the two half maps. For our highest resolution map (4.4 Å closed Pincer-FATKIN, from 3D class A), we have refined the model with restraints against the half1 map. The FSC curves are shown for both half maps. FSC curves for the half1 map and the half2 map (not used for refinement) are nearly identical, suggesting no over-fitting in this resolution range. (**B**) FSC curves for the open models (derived from 3D classes C and D) versus the corresponding unsharpened sum of the two half maps.

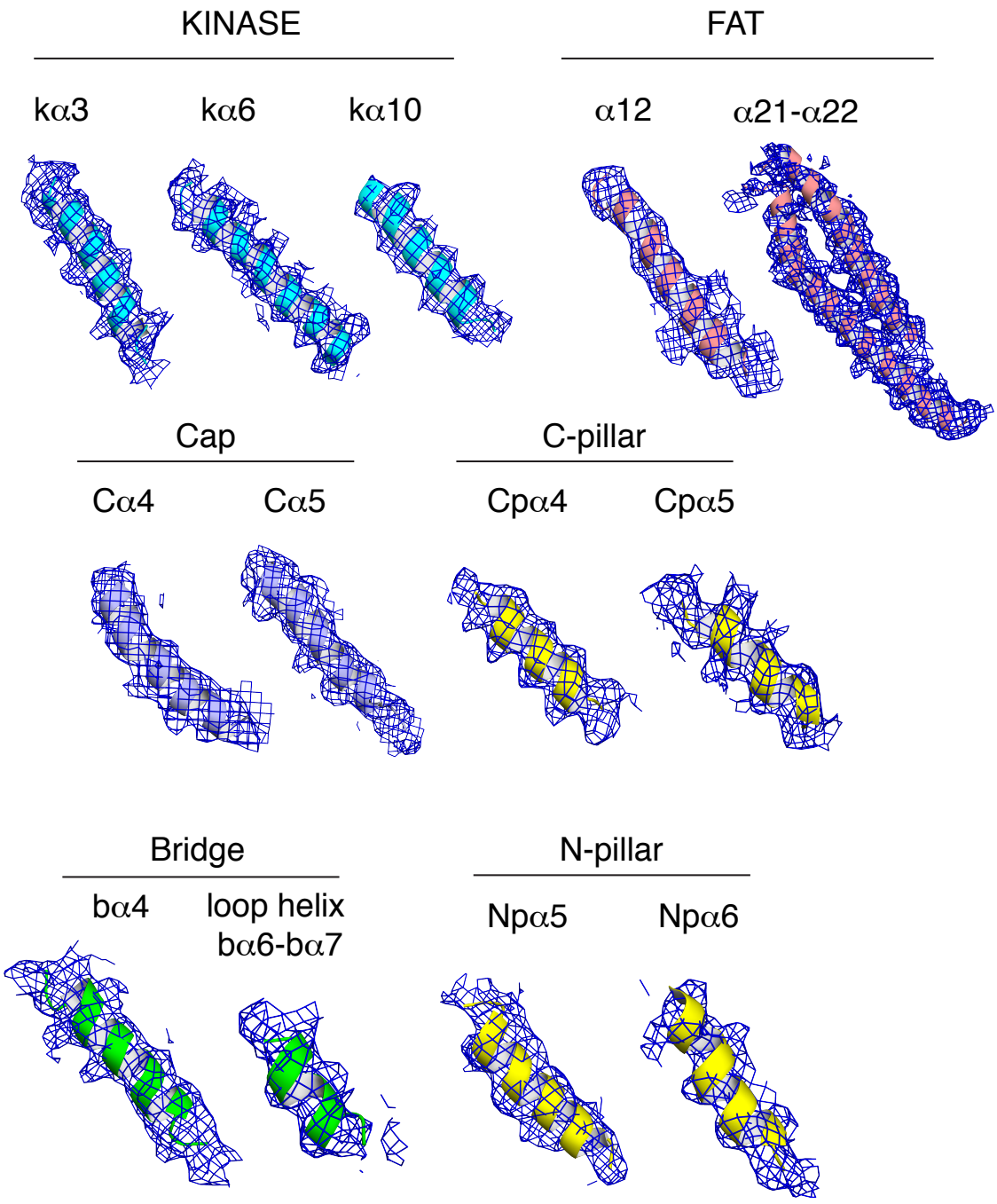

fig. S9. Quality of the density for the highest-resolution human ATM map. In the 4.4 Å resolution map of the closed dimer (derived from 3D class A), helices typically appear as spirals instead of smooth tubes, but the resolution is not, in general, high enough to discern side chains.

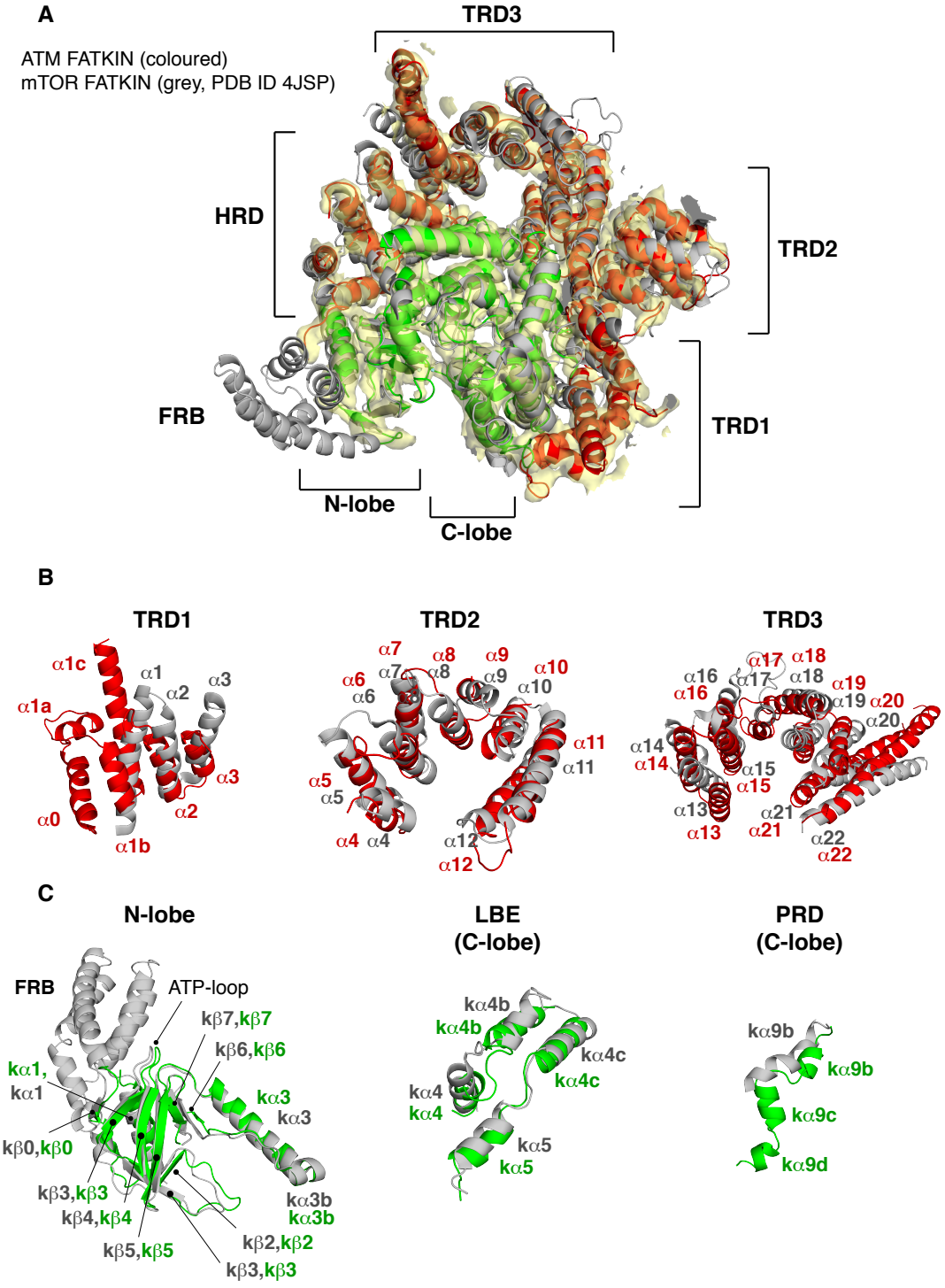

fig. S10. Comparison of the ATM FATKIN with mTOR. (**A**) The FATKIN of ATM superimposed on the mTOR FATKIN (PDB ID 4JSP). The 4.4 Å resolution density for the closed FATKIN is also shown (yellow). (**B**) The FAT domain shows some shifts in TRD1, 2 and 3. TRD1 has three extra helices with respect to the mTOR FATKIN (labeled as helices α0, α1a, α1b; ATM helix α1c corresponds roughly to mTOR α1). TRD2 and

TRD3 have some shifts, but the HRD is essentially identical. (**C**) In the kinase domain, the N-lobe is very similar to the N-lobe of the mTOR FATKIN, apart from the FRB missing in ATM. Although there is no evidence that ATM binds to LST8, the overall conformation of the Lst8-binding element (LBE) is similar to mTOR. The PRD in ATM is more ordered than in mTOR.

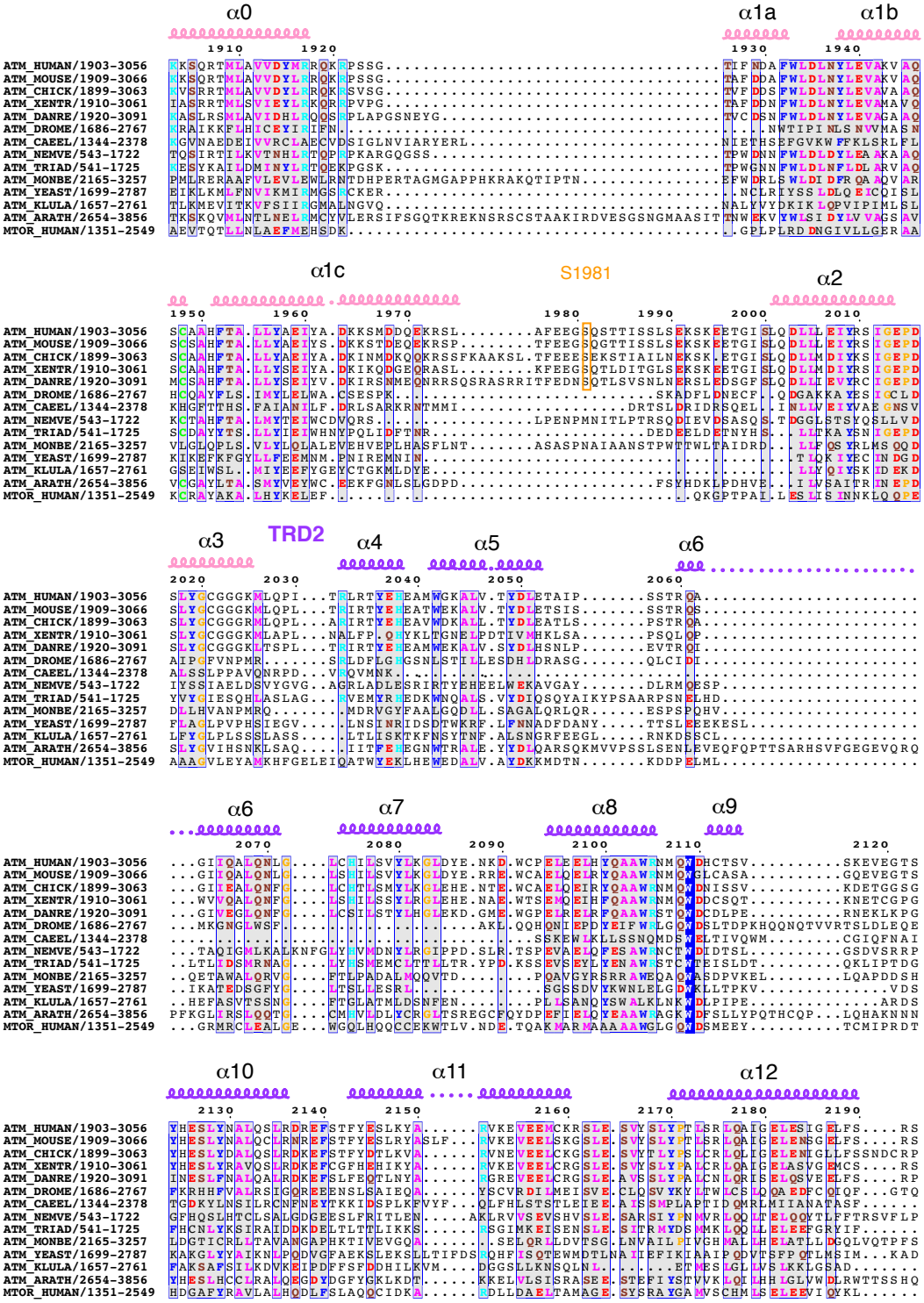
TRD1
α0
α1a
α1b
α1c
S1981
α2
TRD2
α3
α4
α5
α6
α7
α8
α9
α10
α11
α12
ATM_HUMAN/1903-3056
ATM_MOUSE/1909-3066
ATM_CHICK/1899-3063
ATM_XENTR/1910-3061
ATM_DANRE/1920-3091
ATM_DROME/1686-2767
ATM_CAEEL/1344-2378
ATM_NEMVE/543-1722
ATM_TRIAD/541-1725
ATM_MONBE/2165-3257
ATM_YEAST/1699-2787
ATM_KLULA/1657-2761
ATM_ARATH/2654-3856
MTOR_HUMAN/1351-2549

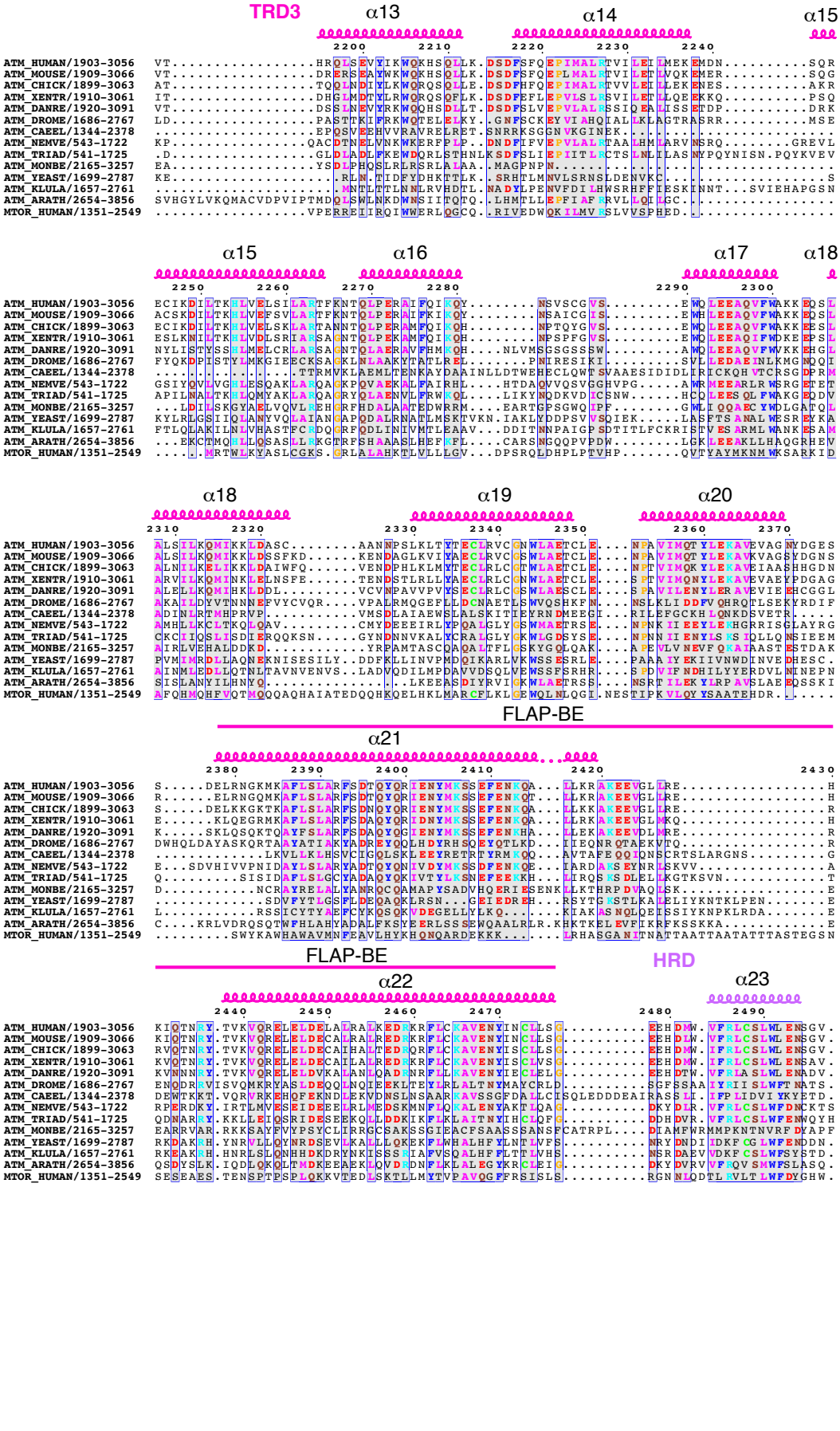
TRD3
α13
α14
α15
α16
α17
α18
α19
α20
FLAP-BE
α21
FLAP-BE
HRD
α22
α23

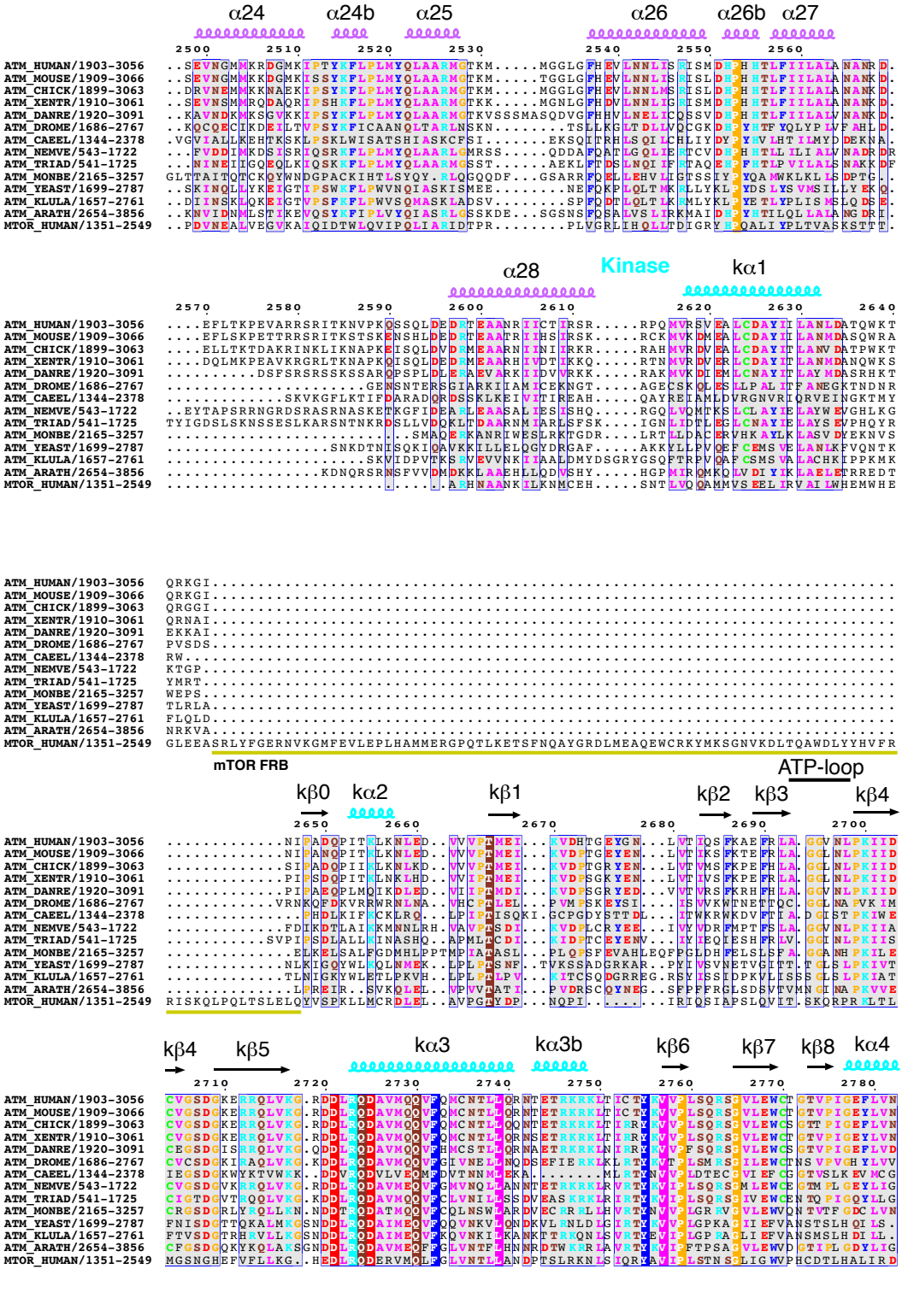
α24
α24b
α25
α26
α26b
α27
α28
Kinase
kα1
mTOR FRB
ATP-loop
kβ0
kα2
kβ1
kβ2
kβ3
kβ4
kβ5
kα3
kα3b
kβ6
kβ7
kβ8
kα4
ATM_HUMAN/1903-3056
ATM_MOUSE/1909-3066
ATM_CHICK/1899-3063
ATM_XENTR/1910-3061
ATM_DANRE/1920-3091
ATM_DROME/1686-2767
ATM_CAEEL/1344-2378
ATM_NEMVE/543-1722
ATM_TRIAD/541-1725
ATM_MONBE/2165-3257
ATM_YEAST/1699-2787
ATM_KLULA/1657-2761
ATM_ARATH/2654-3856
MTOR_HUMAN/1351-2549

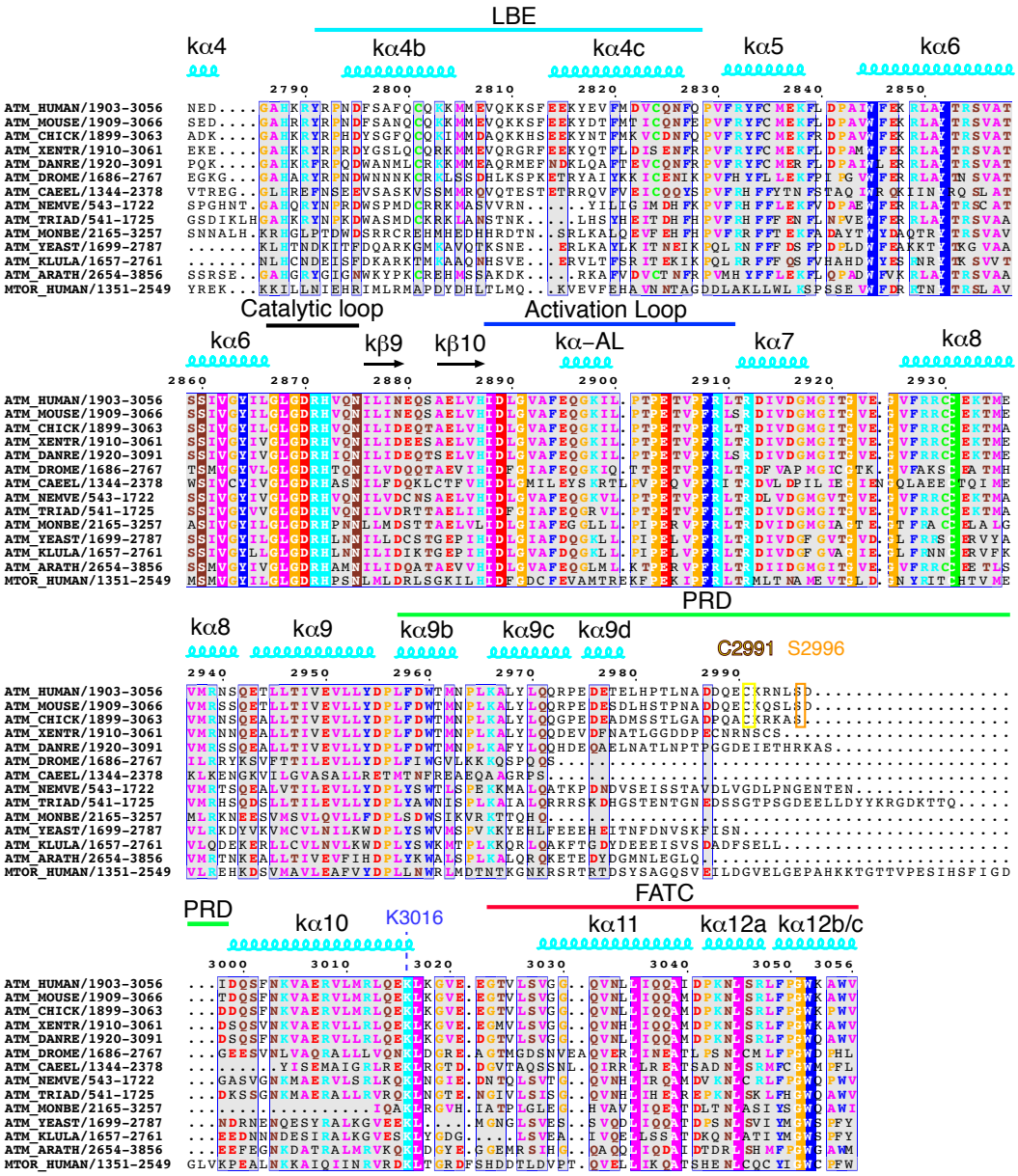

fig. S11. Multiple sequence alignment of the FATKIN regions of human ATM and its representative orthologs, along with that of human mTOR. The representative orthologs span the crown group eukaryotes, i.e. animals, fungi and plants. The initial alignment was constructed using MSAProbs(*54*), which was further refined using HMMER searches(*55*), DSSP secondary structure assignment(*56*) and JPRED secondary structure prediction (*57*) to arrive at the final alignment. The pictorial representation of the alignment was made using ESPript 3.0 server(*58*). The color-coded regions indicate conserved positions and it is clear that the FATKIN regions are conserved across ATM orthologs as well as in human MTOR.

HUMAN	*Homo sapiens* (Human)
MOUSE	*Mus musculus* (Mouse)
CHICK	*Gallus gallus* (Chicken)
XENTR	*Xenopus tropicalis* (Western clawed frog)
DANRE	*Danio rerio* (Zebrafish)
DROME	*Drosophila melanogaster* (Fruit fly)
CAEEL	*Caenorhabditis elegans* (Nematode worm)
NEMVE	*Nematostella vectensis* (Starlet sea anemone)
TRIAD	*Trichoplax adhaerens* (Trichoplax reptans)
MONBE	*Monosiga brevicollis* (Choanoflagellate)
YEAST	*Saccharomyces cerevisiae* (Baker's yeast)
KLULA	*Kluyveromyces lactis* (Candida sphaerica)
ARATH	*Arabidopsis thaliana* (Mouse-ear cress)

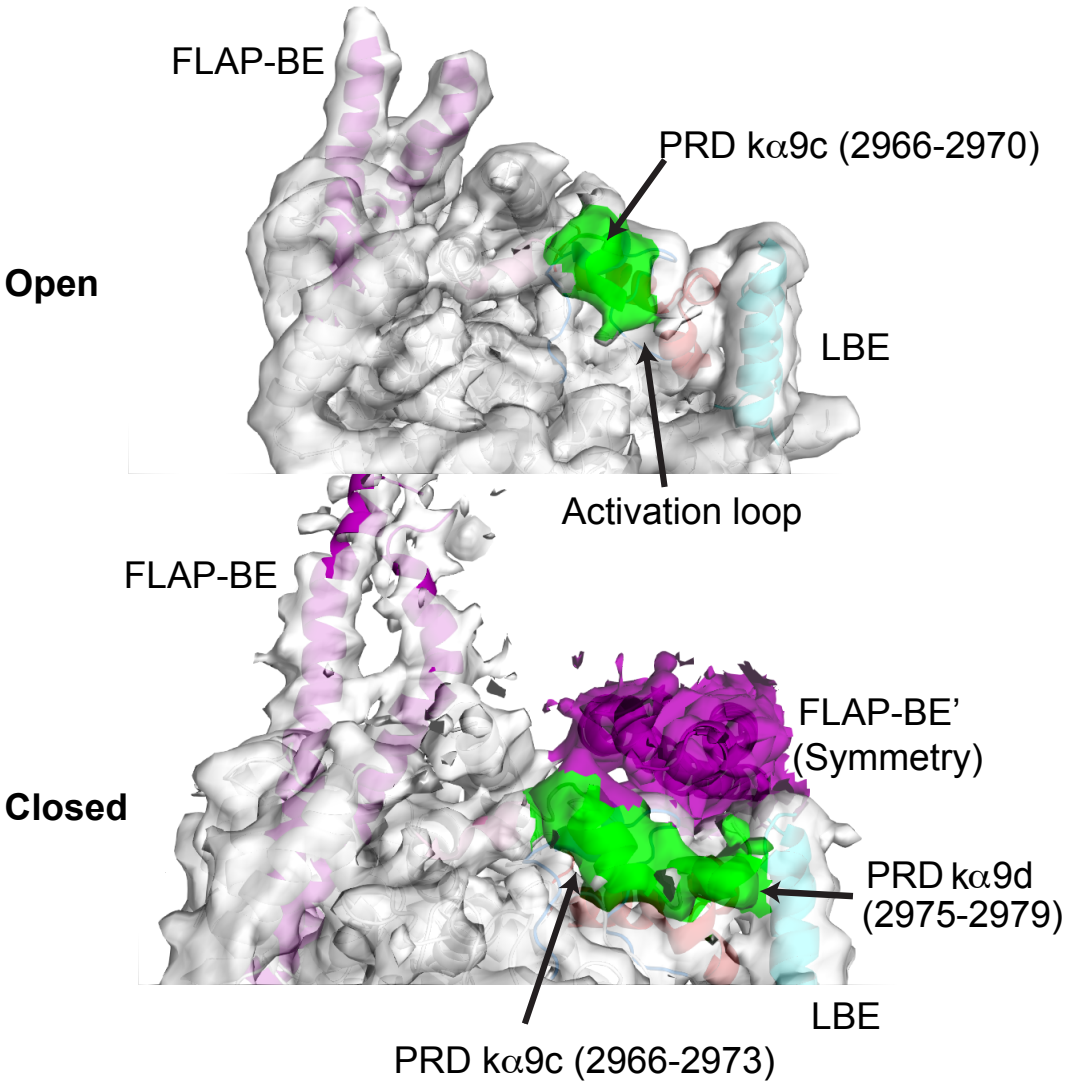

fig. S12. Open and closed conformations of the ATM active site. In the open conformation (upper), the lack of constraint from a symmetry-related FLAP-BE enables the PRD (kα9c, green) to expose access to the active site and the activation loop. In the closed conformation (lower), the FLAP-BE' from the symmetry-related molecule (purple) stabilizes more of the PRD (kα9c and kα9d, green) and restricts access to the active site. Residue numbers of the ordered portions of the PRD are shown in brackets.

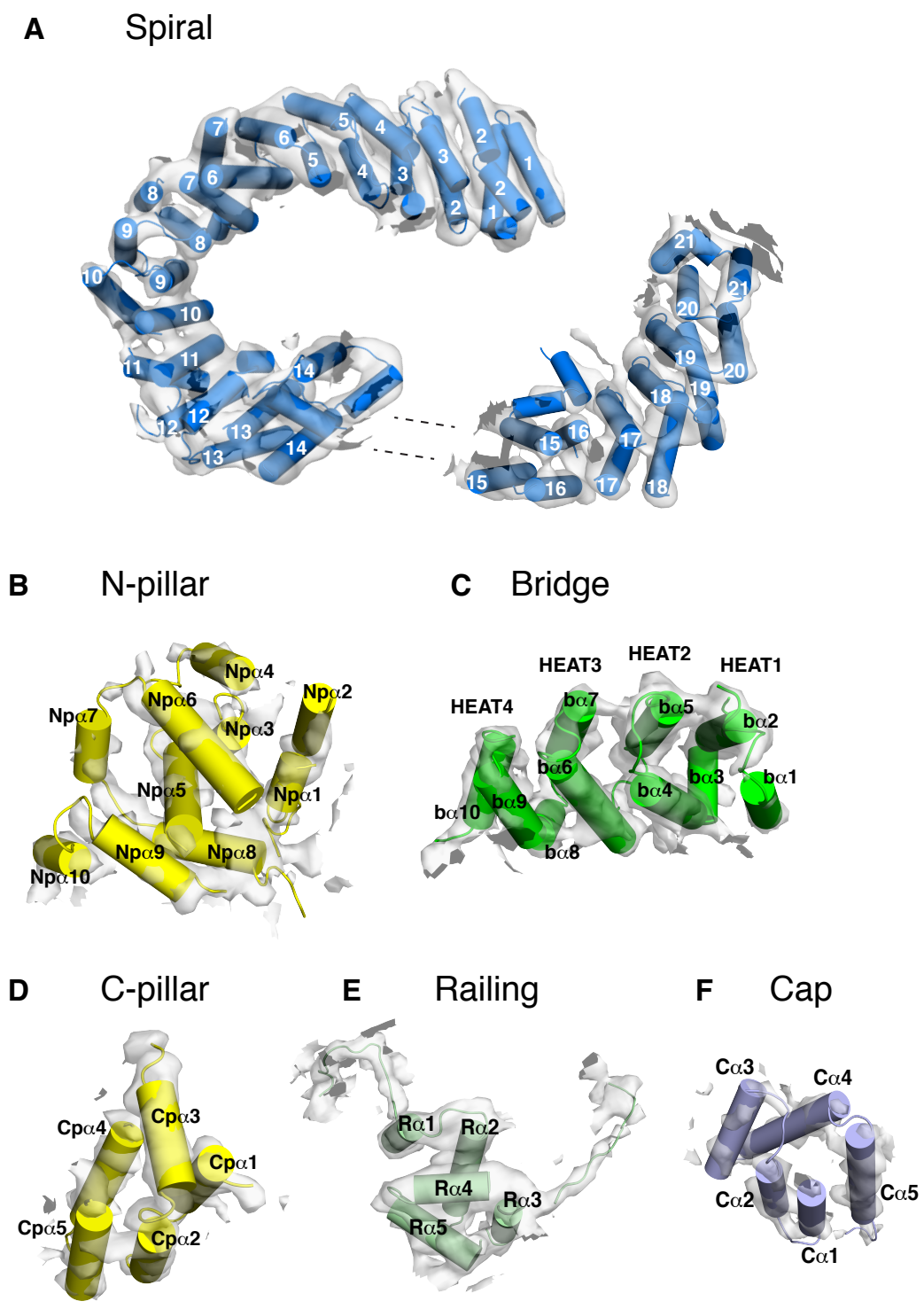

fig. S13. Domains of the N-solenoid of ATM. Close-up views for each of the domains in the 5.7 Å (**A**) and 4.7 Å (**B-F**) resolution maps of the closed dimer. For clarity, the Spiral (**A**) has been broken into two pieces, and it is labelled with numbers indicating HEAT-repeats.

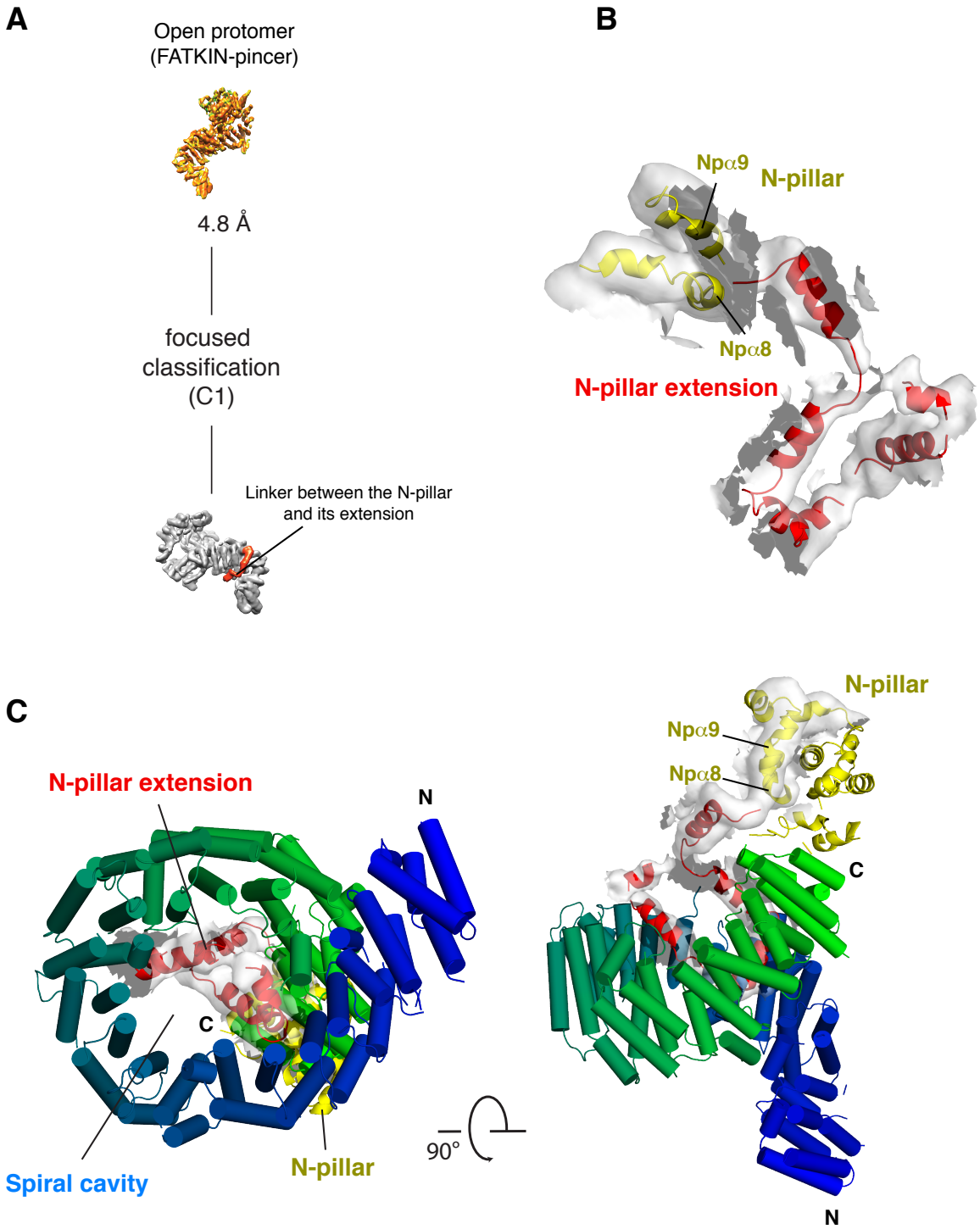

fig. S14. Density bridging the two turns of the Spiral. The highest resolution reconstructions of the closed dimer (from 3D class A) and the open protomer (from 3D classes C and D) both suggest density inside the Spiral that appears to consist of several helices bridging two adjacent turns of the corkscrew-shaped Spiral domain. (**A**) Sub-classification was carried out on the particles used to generate the 4.8 Å resolution open protomer. (**B**) Density from a 12.8k particle sub-class suggests that these helices are part of a larger extension from the N-pillar, however, the connections with the N-pillar are ambiguous. (**C**) Views of the density in the context of the Spiral (colored blue to green from the N- to the C-terminus).

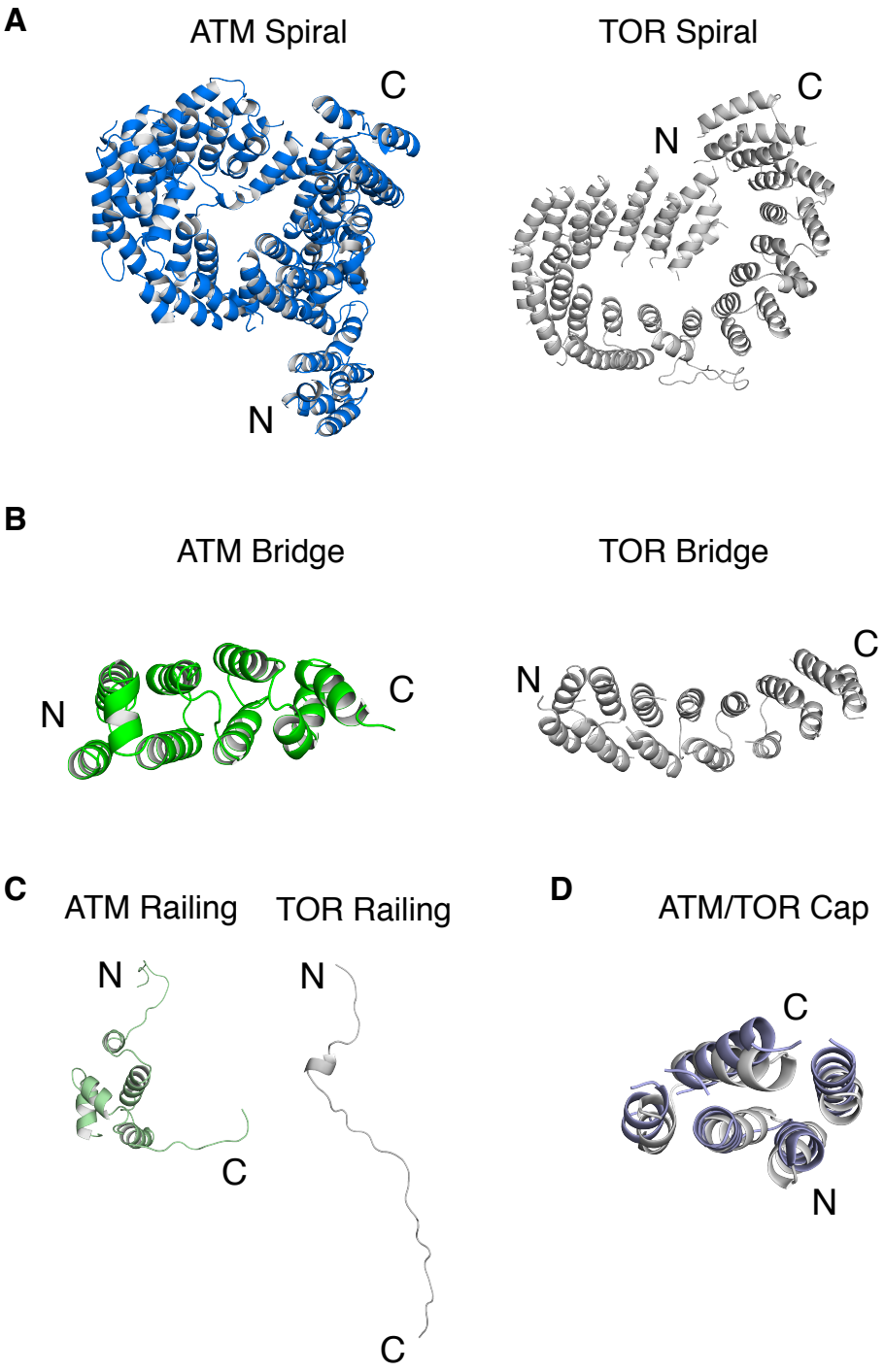

fig. S15. Comparison of structurally conserved domains in the N-solenoids of ATM and TOR. (**A**) The ATM Spiral is shaped like a corkscrew, while the TOR Spiral is more like a flat lock washer. (**B**) The ATM Bridge is made up of HEAT-repeats arranged into a straighter module than the Spiral. The TOR Bridge is much longer than the Bridge of ATM. (**C**) The Railing serves to connect the C-terminal end of the Bridge/C-pillar to the N-terminal end of the Cap. The structures of ATM and TOR Railings are unrelated, but we use the Railing designation only to signify this shared function. (**D**) The Cap domain has essentially the same structure in both ATM (blue) and TOR (grey).

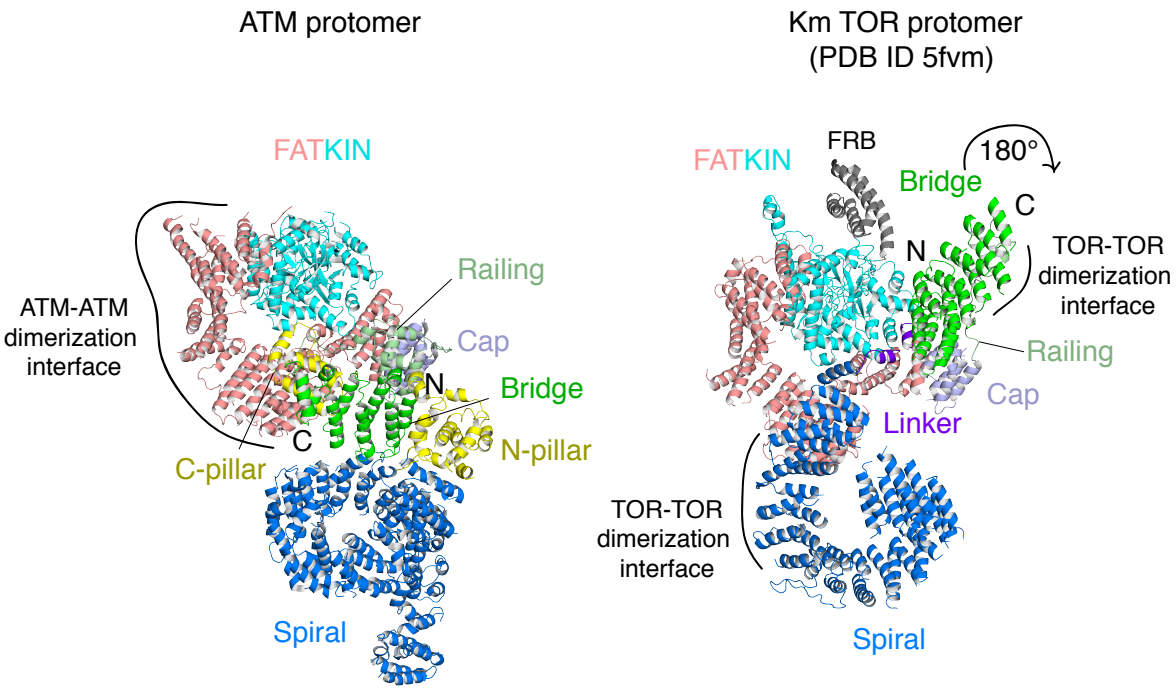

fig. S16. Domain organization of ATM compared with TOR. The FATKIN modules of ATM and TOR are closely related and likely to be similar among all PIKKs. However, TOR and ATM use completely different interfaces to form dimers. Although both ATM and TOR have a Bridge domain, this element is rotated roughly 180 ° in the two structures. Both the fold of the Cap and its relation to the FATKIN are features conserved in the two enzymes.

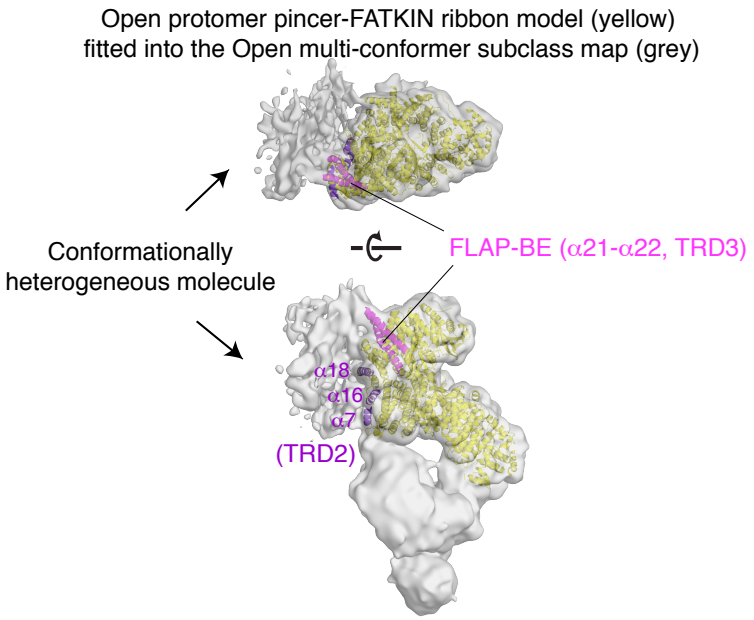

fig. S17. Highest-resolution subclass (8.4 Å resolution) of the open multi-conformer dimer (from fig. S5, 3D class D) has one ordered protomer associated with a weakly ordered second FATKIN. The model for the open Pincer-FATKIN fragment is fit into the density. Interacting helices from TRD2 (α7) and TRD3 (α16, α18) are colored purple, and the FLAP-BE is shown in pink.

table S1. Data collection and refinement statistics.

Data collection parameters for the human ATM				
Dataset	**1**	**2**	**3**	**4**
Grid type	Quantifoil R1.2/1.3 300	Quantifoil R1.2/1.3 300	UltrAuFoil R1.2/1.3 300	UltrAuFoil R1.2/1.3 300
Microscope	FEI Titan Krios	FEI Titan Krios	FEI Titan Krios	FEI Titan Krios
Voltage (keV)	300	300	300	300
Detector	Gatan K2 Summit	Gatan K2 Summit	Gatan K2 Summit	Gatan K2 Summit
Mode	super-resolution counting	super-resolution counting	super-resolution counting	super-resolution counting
Energy filter slit width (eV)	20	20	20	20
Data collection	manual	manual	manual	UCSF Image4
Frames	20	20	20	20
Exposure time (s)	16	16	16	16
Total dose (e-/Å^2)	42	42	42	42
Micrographs[a]	649	832	591	648
Pixel size (Å)	1.43	1.43	1.43	1.43
Box size (Å)	300	300	300	300
Raw particles[b]	108,259	121,876	81,928	59,608
Refinement statistics				
2D-classification[c]		371,671		
3D-classification		139,086		
Species	**closed dimer**	**closed multi-conformer dimer**	**open dimer**	**open multi-conformer dimer**
Final particles	25,315	34,155	15,837	44,719
Final resolution[d]	4.7 Å	8.8 Å	11.5 Å	8.4 Å

[a]number of micrographs used for processing

[b]number of particles extracted after autopicking and manual selection

[c]after final cycle

[d]FSC between two independently refined half-maps, using 0.143 criterion

table S2. Statistics for refined atomic models.

Model	**Closed**			**Open**	
Resolution	4.4 Å	4.7 Å	5.7 Å	4.8 Å	5.7 Å
Ramachandran preferred	88.7%	86.9%	91.7%	92.2%	90.4%
Ramachandran allowed	10.4%	12.9%	8.2%	7.8%	9.3%
Ramachandran outliers	0.89%	0.12%	0.21%	0.06%	0.34%
Correlation (around atoms)	0.83	0.82	0.83	0.85	0.84
RMSD bond lengths (Å)	0.01	0.01	0.02	0.01	0.01
RMSD bond angles (°)	1.25	1.21	1.48	0.91	1.39

movie S1. Open and closed conformations of ATM. The movie is a morph between the open and closed conformations of ATM (created in PyMOL). A peptide substrate (yellow spheres connected by sticks) has been modeled into the open conformation based on the structure of CDK2 bound to a peptide (PDB ID 3QHW). In the closed conformation, the PRD (green) blocks the peptide-binding site. In the open conformation, the PRD moves to enable the peptide bind.